1   **Stand-alone lumbar cage subsidence: a biomechanical sensitivity study of cage design**

2   **and placement.**

3   Andrea Calvo-Echenique[1], José Cegoñino[1], Raúl Chueca[1], Amaya Pérez-del Palomar[1]

4

5   [1]Group of Biomaterials

6   Aragón Institute of Engineering Research (I3A)

7   Department of Mechanical Engineering, University of Zaragoza (Spain)

8   **Corresponding author:**

9   Amaya Pérez-del Palomar

10   María de Luna s/n

11   Departamento Ingeniería Mecánica, Ed. Betancourt, Escuela de Ingeniería y Arquitectura.

12   Zaragoza (Spain)

13   +34 976762872

14   amaya@unizar.es

19
20
21
22
23

24   *1. Abstract and key terms*

25   Background and objective

26   Spinal degeneration and instability are commonly treated with interbody fusion cages either alone or

27   supplemented with posterior instrumentation with the aim to immobilize the segment and restore intervertebral

28   height. The purpose of this work is to establish a tool which may help to understand the effects of intervertebral

29   cage design and placement on the biomechanical response of a patient-specific model to help reducing post-

30   surgical complications such as subsidence and segment instability.

31   Methods

32   A 3D lumbar functional spinal unit (FSU) finite element model was created and a parametric model of an

33   interbody cage was designed and introduced in the FSU. A Drucker-Prager cap plasticity formulation was used

34   to predict plastic strains and bone failure in the vertebrae. The effect of varying cage size, cross-sectional area,

35   apparent stiffness and positioning was evaluated under 500N preload followed by 7.5Nm multidirectional

36   rotation and the results were compared with the intact model.

37   Results

38   The most influential cage parameters on the FSU were size, curvature congruence with the endplates and cage

39   placement. Segmental stiffness was higher when increasing the cross-sectional cage area in all loading directions

40   and when the cage was anteriorly placed in all directions but extension. In general, the facet joint forces were

41   reduced by increasing segmental stiffness. However, these forces were higher than in the intact model in most of

42   the cases due to the displacement of the instantaneous centre of rotation. The highest plastic deformations took

43   place at the caudal vertebra under flexion and increased for cages with greater stiffness. Thus, wider cages and a

44   more anteriorly placement would increase the volume of failed bone and, therefore, the risk of subsidence.

45   Conclusions

46   Cage geometry plays a crucial role in the success of lumbar surgery. General considerations such as larger cages

47   may be applied as a guideline, but parameters such as curvature or cage placement should be determined for each

48   specific patient. This model provides a proof-of-concept of a tool for the preoperative evaluation of lumbar

49   surgical outcomes.

50   Key terms: Finite element model, stand-alone intervertebral cage, parametric model, subsidence, stability.

51

2. *Introduction*

Spinal degeneration and instability are commonly treated with interbody fusion cages either alone or supplemented with posterior instrumentation. The aim of this surgery is to stabilize the segment and restore intervertebral height. Lumbar cages are widely employed in combination with additional screw instrumentation to ensure segment immobilization and avoid the risk of non-union. However, although widely accepted as a successful treatment, this additional fixation, apart from being more invasive, has been reported to present some complications such as screw loosening or implant failure. Besides, some biomechanical studies have suggested that lumbar intervertebral disc (IVD) cages are sufficiently stable to be used as stand-alone devices [1], provided that they are introduced using a minimally invasive technique that ensures preservation of important stabilizing structures [2,3]. Large scale clinical studies have also demonstrated no differences in clinical outcomes between patients with stand-alone cages versus those with additional posterior fixation [4]. Although instability was initially defined as a loss of stiffness, and later as a reduction of the neutral zone [5], it is generally accepted that instability is associated with an abnormal load pattern which not necessarily would imply an increase in segmental movement as occurs during disc degeneration [6]. For that reason, and given that the fusion surgery aims to reduce the movement, throughout this paper the outcomes would be discuss in terms of segmental stiffness, directly related with the relative movement of the segment.

The use of stand-alone cages has shown to be very controversial presenting several problems chief of which is the risk of subsidence of the device into the bone owing to the high contact pressures on the bony endplates. For this reason, this study was focused on the investigation of possible factors which may contribute to reduce this risk in cages placed as a stand-alone construct. Although subsidence in early postoperative stage may increase the contact area, avoid the peak pressures caused by irregularities and prevent the progression of subsidence, high-grade subsidence can lead to a reduction in the intervertebral space height [7]. Thus, the use of an appropriate constitutive material of the vertebral bone incorporating a plasticity formulation would lead to a better prediction of the risk of subsidence in a stand-alone fashion. Previous studies have used Von Mises equivalent stress as the criterion for bone yielding [8,9]. However, considering that bone should be treated as a brittle material, the Von Mises criteria would not be suitable [10]. In this study, we used the modified Drucker–Prager Cap model, which takes the contribution of hydrostatic stress into consideration, as the yield criterion to model the inelastic behaviour at a continuum level.

80 On the other hand, cage characteristics such as shape, material and positioning are also expected to have a

81 significant influence on surgery success. Previous studies have used finite element (FE) models to compare

82 among commercial cages, but only some of them have discussed the influence of cage material [11] or shape

83 [8,12] using parametric or optimization methods. In their study, Hsu et al.[12] used a genetic algorithm to find

84 the cage shape with an optimal subsidence resistance. However, they assumed flat endplates instead of real

85 geometry which may lead to a more uniform pressure distribution and an underestimation of subsidence risk.

86 Later on, a study comparing a standard cage with a custom-fit one showed that patient-specific cage geometry

87 could reduce the stress concentration on the endplates [8]. However, these studies provided a limited prediction

88 of subsidence as they used elastic material models.

89 In this study we aimed to prove a model which will serve as a tool for the preclinical evaluation of surgery

90 outcomes that any interbody device or supplementary fixation may have in each specific patient. Particularly, in

91 this work, the influence of different design parameters and positioning of a bean-shaped cage on segment

92 stiffness and subsidence risk has been studied. The selection of a stand-alone device responds to the higher risk

93 of subsidence reported for this technique but in no case it is aimed to show a comparison with additional

94 instrumentation or to demonstrate a superiority of one technique over the other. To this end, we conducted a

95 parametric FE analysis of a cage design of varying size, cross-sectional area and position, and evaluated it in a

96 patient-specific functional spinal unit (FSU). The main contribution of this study is the evaluation of cage

97 subsidence with an elasto-plastic material formulation with different behaviour for traction and compression for

98 the bone. In addition, this formulation accounted not only for the stresses over the yield stress limit, but also

99 considered the hardening of the material.

100

3.   Materials and Methods

102   A 3D FE model of a FSU was developed to evaluate the influence of cage design and positioning in the surgical

103   outcome. Firstly, the intact segment was simulated and validated to set a control scenario. Then, the elements

104   corresponding to the nucleus and inner annulus were removed to place a stand-alone cage. A total of 50 models

105   were built (intact FSU + cage with neutral parameters + 8 variations of each parameter) as explained below.

106   *FSU finite element model*

107   A L4-L5 FSU was modelled including vertebral bodies, annulus fibrosus, nucleus pulposus, cartilaginous

108   endplates, facet joints and the seven major ligaments. This model will be referred in the following as intact

109   model. The vertebral bodies were segmented from a computed tomography of an asymptomatic 46-year-old male

110   subject [13] and divided into a 0.5mm thick cortical layer [14] meshed with one layer of hexahedral elements

111   and the cancellous bone, meshed with tetrahedral elements of 2mm mean size due to the geometrical

112   irregularities. Bone was characterized as a transversal isotropic material with a Druker Prager cap plasticity

113   formulation (see Online resource 1). Soft tissues were modelled according to anatomical characteristics: the

114   annulus fibrosus and the endplates were meshed with linear hexahedral elements with mean mesh size of 1.5mm.

115   For the annulus fibrosus (AF) an anisotropic material with two families of fibres (±30º), using the Holzapfel

116   strain energy function, was used [13]. While, the endplates were characterized as linear elastic material. The

117   nucleus pulposus was meshed with hexahedral elements and characterized as a non-linear NeoHookean material.

118   The spinal ligaments were modelled as uniaxial truss elements with strain-dependent behaviour under traction

119   and without resistance to compression. Finally, the facet joints were modelled as 0.2mm thickness cartilage with

120   a frictionless surface-to-surface contact combined with a penalty algorithm for normal contact (200 N/m

121   stiffness, initial gap of 0.4mm) [15]. All mechanical properties are summarized in Table I. To obtain the ideal

122   size of the FE mesh (shown in Figure 1), a process of mesh refinement was executed until verifying mesh

123   convergence. The mesh refinement process was stopped when the difference between the results was 5% or

124   lower. This analysis gave a global mesh size which is summarized in Table II.

125   *Cage design and parameterization*

126   The intact model described previously was modified to introduce the cage. Thus, the elements corresponding to

127   the nucleus pulposus and inner annulus were removed to host the cage. After the insertion, the empty region left

128   between the annulus and the cage was filled with tetrahedral elements simulating the granulation or

129   inflammatory tissue (its mechanical properties are shown in Table I). Furthermore, simulating a minimally

130   invasive surgery, the ligaments were considered to remain intact.

131   A parametric model of a bean-shaped cage was created using Python scripting in ABAQUS 6.13 (SIMULIA,

132   Providence, RI, USA) (Figure 1a). The cross-sectional area of the cage was varied by modifying the axes

133   distance (length), radius (width) and thickness (Figure 1a) to investigate the influence of the apparent stiffness of

134   the cage. On the other hand, the curvature of the cage ends, which will contact the top and bottom vertebral

135   endplates, was varied from flat to high convexity to account for the effect of geometry congruence (Figure 1b).

136   This parameter was defined as the difference in percentage between the central and lateral cage height. An

137   additional transversal hole was included varying its height because, despite it is very common in commercial

138   cages to promote bone growth around the implant, it modifies the cage stiffness (Figure 1b). Finally, the cage

139   was placed at a central position and moved along the antero-posterior direction as shown in Figure 1c. The

140   election of the parameters to be varied responds to the clinically reported influence of cross-sectional area and

141   cage positioning on surgery outcome [7,16–18]. The neutral parameter values were set in accordance to the

142   standard shape of commercial implants. Then, one parameter was varied at a time while maintaining neutral

143   values for all other parameters. The upper and lower limits and the neutral values for each parameter are

144   summarized in Figure 1a, 1b and 1c. Each parameter has been varied uniformly between minimum and

145   maximum values with a total of 9 values per parameter. The cage was meshed with linear hexahedral elements

146   after a sensitivity mesh analysis (0.7mm size) and made of PEEK (Table I). A surface-to-surface contact with a

147   friction coefficient of 0.5 was assigned to the cage-endplate interface [18]. The penetration of the cage into the

148   granulation tissue was avoided with a normal non-penetrating contact.

149
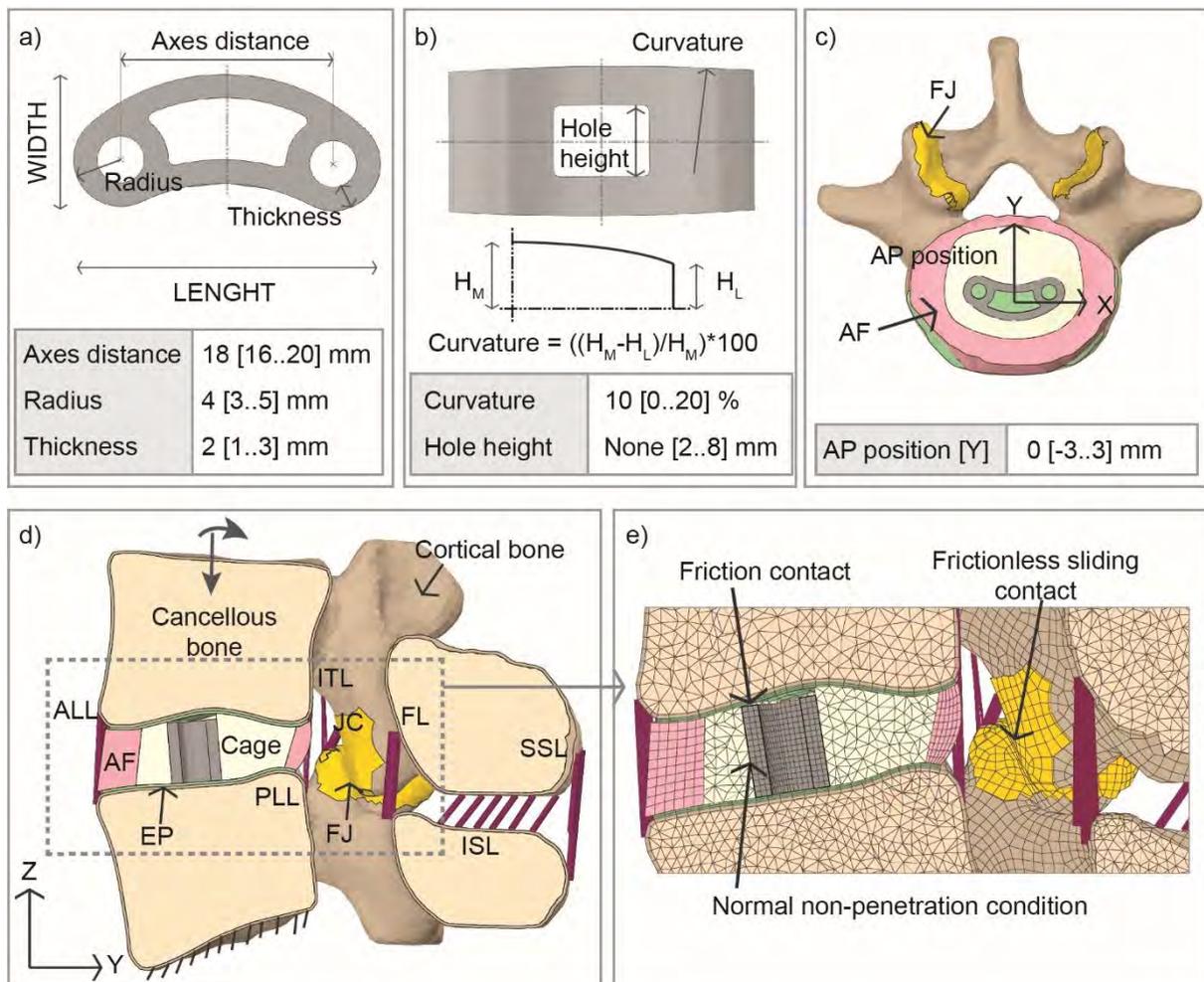
Fig 1 a) Design parameters to vary the cross-sectional area of the cage; b) Design parameters to vary the congruence of the ends in contact with the vertebrae (curvature), defined as the percentage of the difference between the central (H_M) and the lateral (H_L) height of the cage, and a transversal hole (7mm width) with a modifiable height; c) Cage placement on L5 vertebra, the cage was moved along the antero-posterior direction. Granular tissue was considered between the annulus fibrosus (AF) and the cage. The facet joint (FJ) cartilage of L5 is shown; d) FSU model including cortical and cancellous bone, endplates (EP), annulus fibrosus (AF), ligaments [anterior longitudinal (ALL), intertransverse (ITL), posterior longitudinal (PLL), capsular (JC), flaval (FL), interspinous (ISL) and supraspinous (SSL)], facet joints (FJ) and interbody cage. All movements were constrained in the lower portion of L5 and the load was applied in the center of L4; e) Details of the mesh and contact definitions of the FE model.

162

163 **Table I**. Material properties of the FSU components. ε_{12} defines the strain point at which the bi-linear elastic

164 stress-strain curve change its slope from E_1 to E_2. *(PEEK-OPTIMA®, Invibio™ Biomaterials Solutions)

165 +Nucleus tissue only exists in the intact FSU model, while granular tissue is only present in the operated FSU.

	Young modulus [MPa]	Poisson coef.		Yield stress [MPa]	Ultimate yield strain [%]
Cortical bone [19,20]	$E_{XX} = E_{YY} =11300$ $E_{ZZ} = 22000$	$\nu_{XY} = 0.0484$ $\nu_{YZ} = \nu_{XZ} = 0.203$	Tension	155	-
	$G_{XY} = 3800$ $G_{YZ} = G_{XZ} = 5400$		Compression	173	
Cancellous bone [19,21]	$E_{XX} = E_{YY} =140$ $E_{ZZ} = 200$	$\nu_{XY} = 0.045$ $\nu_{YZ} = \nu_{XZ} = 0.315$	Tension	1.75	1.59
	$G_{XY} = G_{YZ} = G_{XZ} = 48.3$		Compression	1.92	1.45
Endplates [19]	$E = 23$	$\nu = 0.4$			
Facet joints [15]	$E = 35$	$\nu = 0.4$			
Granular tissue [22]±	$E = 0.2$	$\nu = 0.167$			
Cage (PEEK)*	$E = 4100$	$\nu = 0.36$		100-115	
	C_{10} [MPa]	D [MPa^{-1}]	K_1[MPa]	K_2	
Annulus [23]	0.34	0.306	1.8	11	
Nucleus [24]±	0.16	0.024	-	-	
Ligaments [25,26]	E_1 [MPa]	E_2 [MPa]	ε_{12}	Number of elements	Area [mm²]
ALL	7.8	20.0	0.12	10	32.9
PLL	1.0	2.0	0.11	9	5.2
LF	1.5	1.9	0.062	6	84.2
ITL	10.0	59.0	0.18	16	1.8
SSL	3.0	5.0	0.2	4	25.2
	Stiffness [N/mm]		ν	Number of elements	Area [mm²]
JC	30.6 ± 1.5		0.4	14	43.8
ISL	8.7 ± 6.5		0.4	11	35.1

166

167

168 **Table II.** Mesh details. The granular and cage parts had different number of elements depending on the cage
169 shape and are not listed within the table.

	ELEMENT TYPE	NUMBER OF NODES	NUMBER OF ELEMENTS
CORTICAL BONE	Hexahedral	32474	16432
CANCELLOUS BONE	Tetrahedral	63148	331542
ANNULUS FIBROSUS	Hexahedral	5216	4032
NUCLEUS PULPOSUS	Hexahedral	2664	2128
ENDPLATES	Hexahedral	5574	3520
FACET JOINTS	Squared membrane	921	817
LIGAMENTS	Truss	72	36

170
171
172
173 *Boundary conditions*

174 Firstly, the intact FSU was validated using previous in-vitro and computational studies [27,28]. Thus, a

175 compressive load of 100N followed by a 7.5Nm moment in different directions was introduced and the obtained

176 range of motion (ROM) was compared with the results available in the literature.

177 Afterwards, a physiological loading scenario was introduced. A compressive follower preload of 500N [29] was

178 applied between the vertebral centres without any derived rotation. Then, a ±7.5Nm [30] moment load in

179 flexion-extension, lateral bending and axial rotation at the centre of L4 was applied while movement at the lower

180 portion of L5 was restricted. These conditions were applied to the intact FSU, as well as to the FSU with each

181 cage design.

182   4.   Results

183 *Intact FSU validation*

184 The ROM of the intact FSU was validated by comparison with in-vitro [27] and computational data [28] from

185 literature. In Figure 2, the rotation of the intact FSU for every movement is compared with data in the literature,

186 and a good result was achieved for every case. Notwithstanding the fact, that the variability obtained by Heuer

187 and collaborators [27] is very high, our results also fall in the range of the computational analysis made by

188 Zander and collaborators [28].
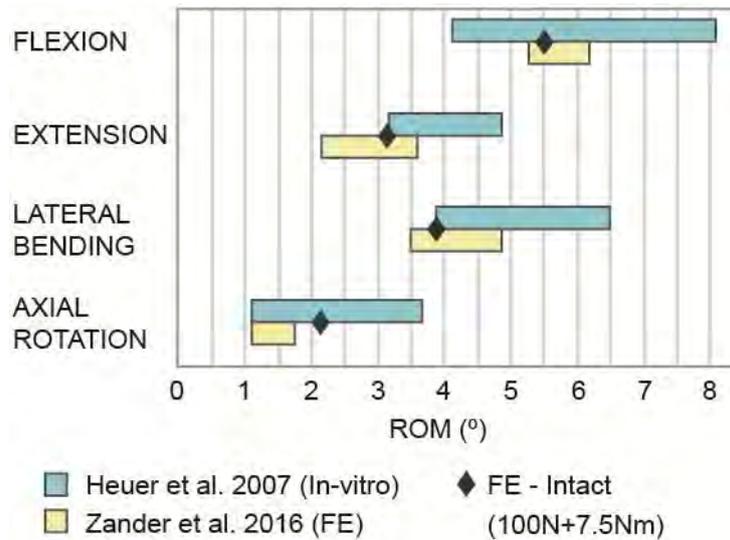
Fig 2. FSU ROM validation by comparison with previous in-vitro and computational models of L4-L5 segment.

Segmental stiffness

As it has been mentioned in the Introduction section, the segmental stiffness is directly related with the relative movement of the segment. For the same applied moment, an increase in the movement of the segment will imply a decrease in segmental stiffness. Thus, in this section, the ROM of the FSU for each cage design and position is compared with the rotation of the intact segment. In Figure 3, it can be seen that the parameters exerting the strongest effects were radius and antero-posterior position.

In this work it was assumed that a decrease in segmental stiffness with respect to the intact model would be undesirable for two reasons. Firstly because the aim of the surgery is to promote fusion with the consequent immobilization. And secondly, because an excessive motion could induce problems in the neighbouring structures. The segmental stiffness was increased by increasing the radius, which means a wider cage, in all loading directions. A longer cage, increasing the axes distance, led to a stiffer segment in extension and lateral bending while a higher curvature led to the opposite outcome. In addition, in axial rotation a flat cage reduced the segmental stiffness more than a biconvex one. On the other hand, the antero-posterior positioning of the cage had a different impact depending on the load direction: an anteriorly placed cage increased the segmental stiffness in flexion, lateral bending and axial rotation but decreased it in extension. However, an extreme posterior placement also increased the rotation in extension.
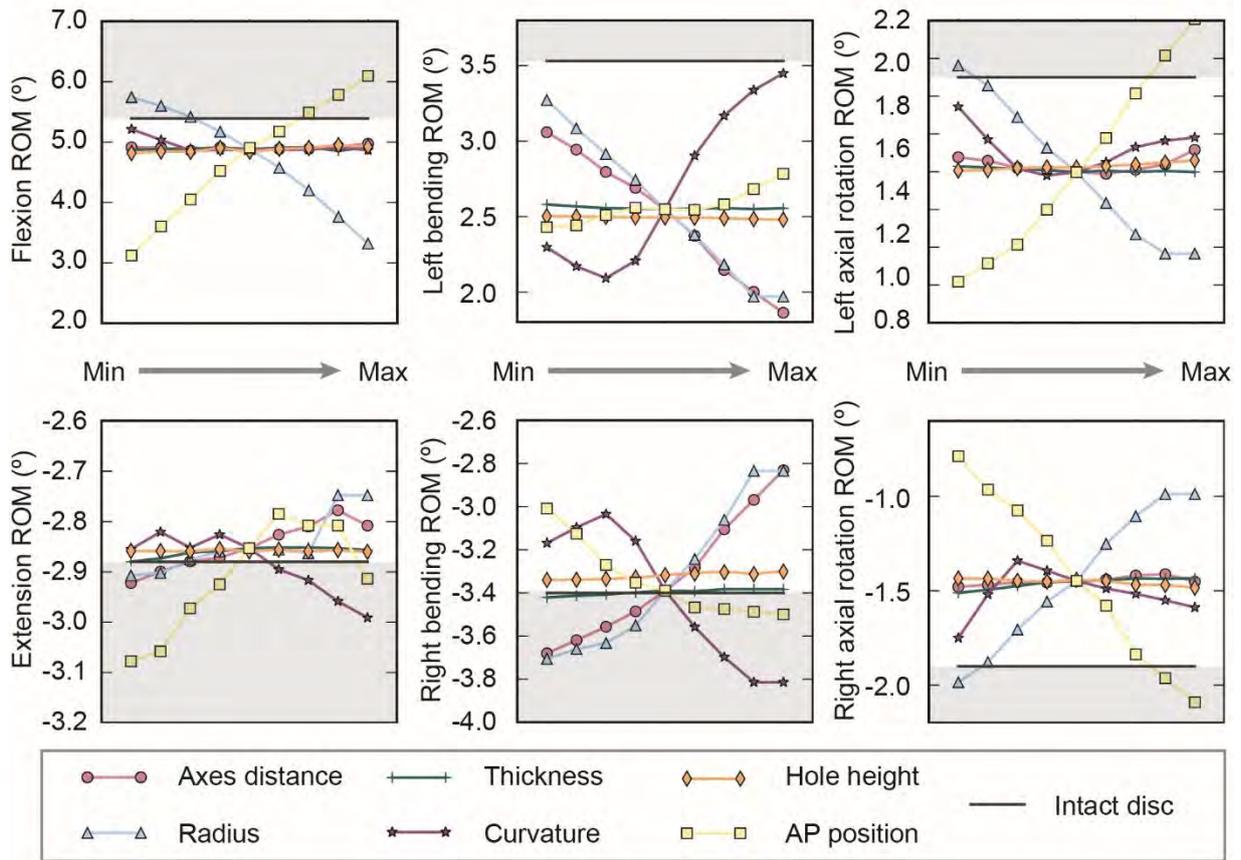
Fig 3 Change of the final rotation of the FSU due to the variation of each parameter in flexion, extension, lateral bending (LB) and axial rotation (AR). The rotation of the intact segment under the same conditions is shown as reference. The shaded area denotes the ROM for which the segment would loss stiffness.

Facet joint forces

In flexion, the facet joints remained unloaded for the intact model. However, the presence of a cage led to the appearance of facet forces, which were not significant in comparison with those depicted in Figure 4 for extension, lateral bending, and axial rotation. As mentioned before, short cages and high curvatures caused an increase of the segment movement increasing the facet forces more than 20% in extension and lateral bending, and more than 30% in axial rotation. On the contrary, a drastic reduction of the facet forces was obtained when the cage was posteriorly placed because most of the load was transmitted through the endplates instead of through the posterior elements. Although in general, a higher segment stiffness was accompanied by a facet force reduction, this force was in many cases higher than in the intact segment. This increment is related to the displacement of the instantaneous centre of rotation (ICR).
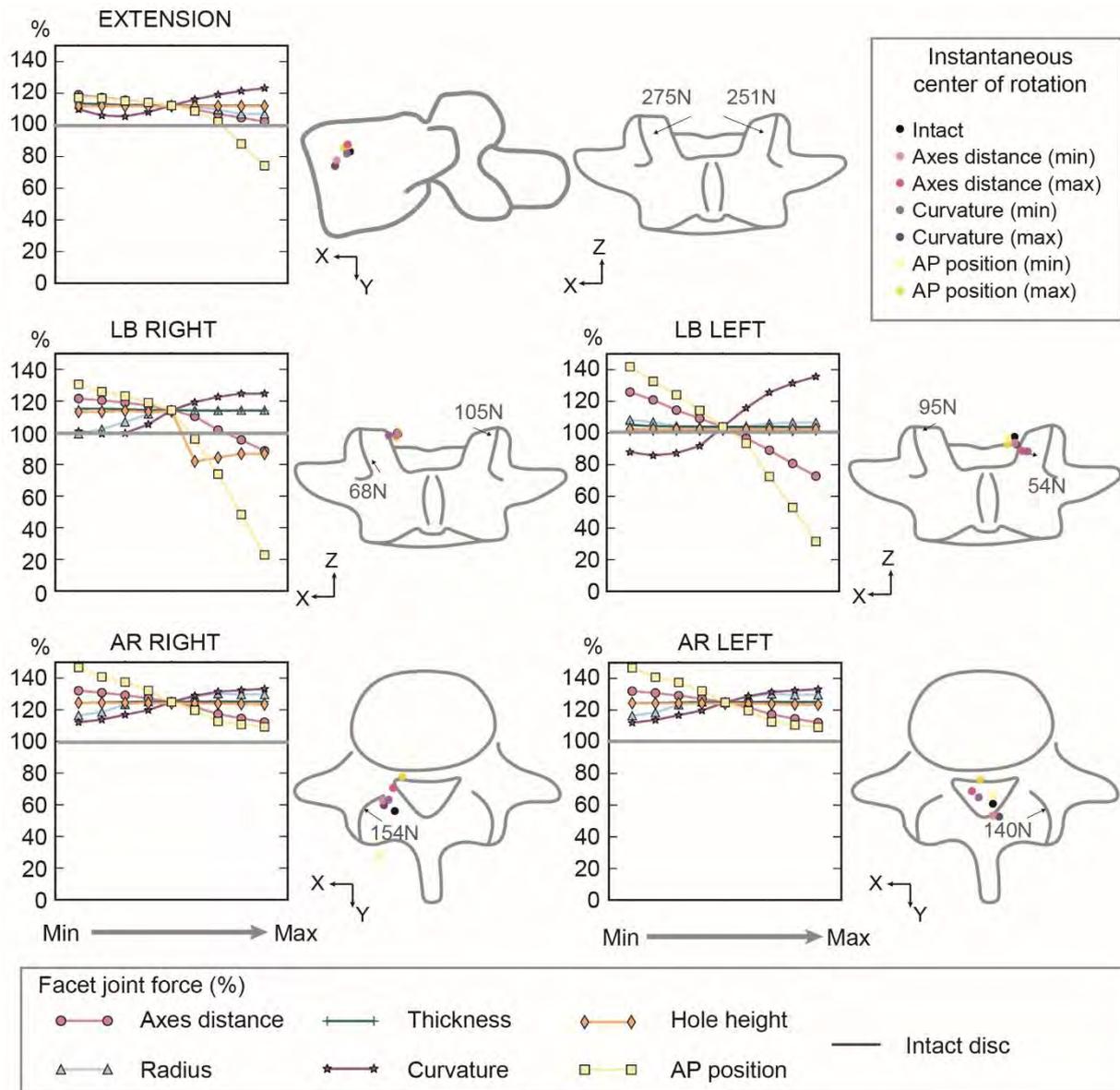
Fig 4 Change in the force supported by the most loaded facet joint due to the variation of each parameter under extension, lateral bending (LB) and axial rotation (AR) in percentage of the intact force. At the right of each graph, the scheme of L5 has been depicted with the direction and value of the facet joint forces in the intact FSU. The instantaneous center of rotation has been plotted for the intact case, and the maximum and minimum values of the parameters which affect the most the facet joint forces (axes distance, curvature and AP position).

*Risk of cage subsidence*

After a careful analysis of the results, it was observed that the maximum contact pressures appeared for flexion and lateral bending movements at the bottom endplate. Due to the irregularities of the endplate geometry, these

233   peak pressures took place on small areas and did not follow a uniform trend with the variations of the

234   parameters. Therefore, the nominal contact pressures were analyzed. Once again, flexion and lateral bending

235   transmitted the highest forces through the endplates and: radius, curvature and anteroposterior positioning,

236   exerted the greatest influence. Regarding the bone integrity, it was observed that these parameters also had the

237   greatest influence in the appearance of inelastic strains. Furthermore, caudal vertebra presented a higher volume

238   of failed bone. Here the most significant results are shown; more details can be found in the Online resource 2.

239   Figure 5 depicts the change in bone volume that had undergone inelastic strains with the most influential cage

240   parameters. In flexion, it was observed that a cage with a curvature higher than 12.5% or a radius higher than

241   4.25mm caused bone failure preceding cage subsidence. In turn, an anteriorly placed cage also led to bone

242   failure.

243   On the other hand, in extension, the yield zone moved backward to the vertebral arch and the facet joints, where

244   the inelastic strains in the arch were primarily caused by tensile stresses due to the contact between the facet

245   joints. Furthermore, plastic strains on the endplates were obtained with a posterior positioning of the cage.

246
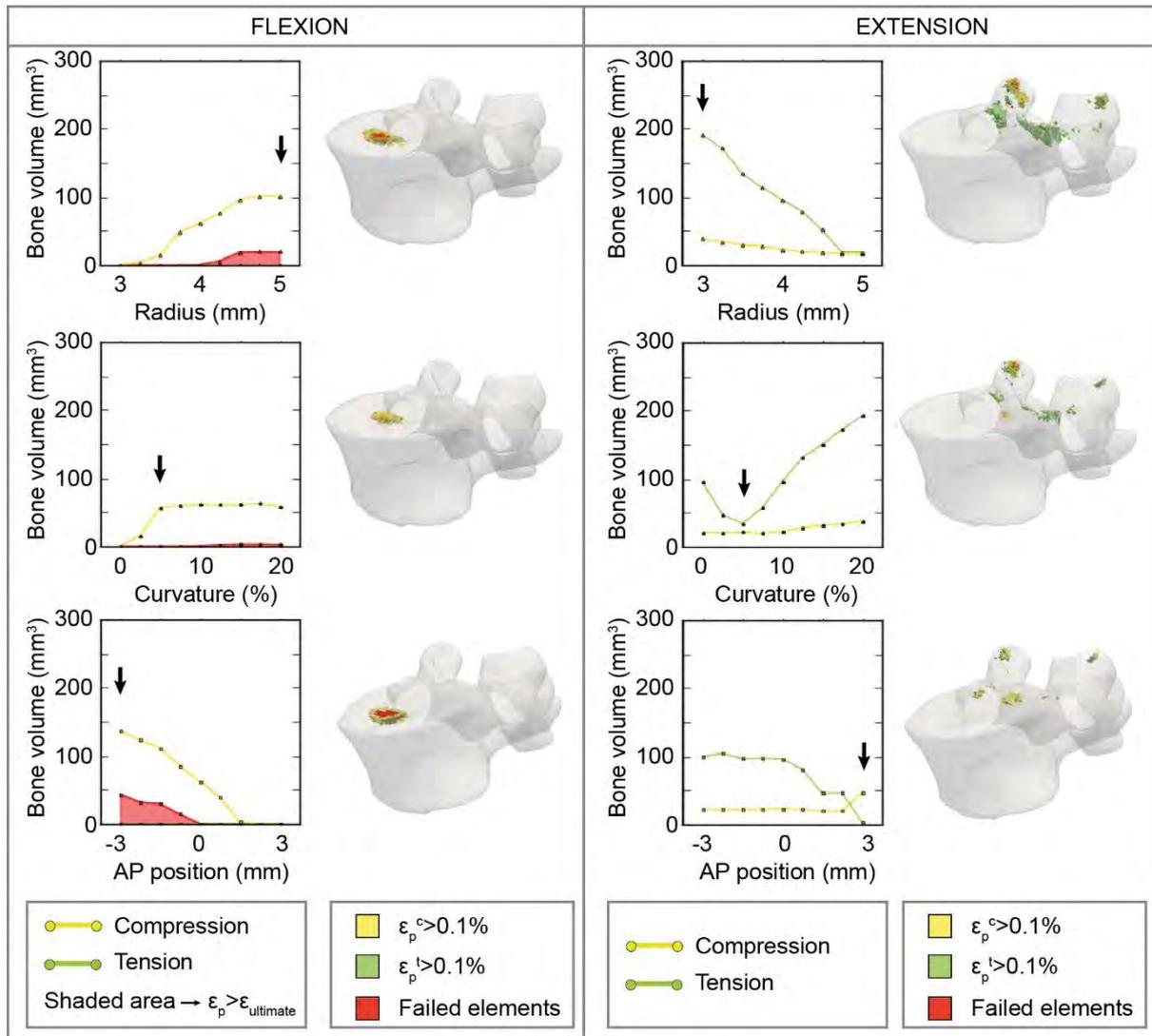
Fig 5 Change in the bone volume that undergone plastic strains due to the variation of radius, curvature and AP position. ε_p^c and ε_p^t are the plastic strains in compression and tension respectively (see Table I). The volume of failed bone has been represented as a shaded area. At the right of each graph, the distribution of plastic strain is shown in L5 for the case marked by the arrow.

5. Discussion

In this work, the effect of varying interbody cage design and placement on segmental stiffness and risk of subsidence has been studied using FE models with a post-yield characterization of the vertebral bone. Because the main goal of this work was to provide a useful tool for preoperative evaluation: range of motion, facet forces and bone integrity have been studied as key factors to achieve a successful fusion surgery.

Historically, supplementary fixation has proved to provide greater stability, however, recent clinical studies have shown successful fusion using stand-alone cages [2,4]. In this study, a stand-alone cage was tested using a patient specific geometry and the segmental stiffness based on the ROM was compared with an intact segment. Thus, higher segmental stiffness was predicted for wider and longer cages (high cross-sectional area) in agreement with in vitro and clinical findings [7,31]. Nonetheless, the maximum cage width would be ultimately determined by the risk of neural injury during the insertion. Cage placement has also demonstrated a high impact in segmental stiffness. As seen in clinical practice an anterior positioning of the cage makes for a stiffer construct [16]. In our study, all rotations were reduced when the cage was anteriorly placed except for extension movement. Similarly, previous studies reviewed elsewhere [32] have shown greater range of motion in extension. In these studies, the loss of stiffness may be caused by the removal of stabilizing structures such as ALL and facet joints while, here, these structures were preserved, simulating a minimally invasive surgery, and allowed to achieve a stiffer construct by varying the device design and placement.

Besides, an alteration in the load transmission through the posterior elements was observed with the variation of the interbody cage design. Our results showed that, the higher the segmental stiffness achieved, the less the forces at the facet joints, except for position variation. However, facet forces were higher than the intact ones for most of the analysed cases, which seems to be inconsistent with the idea of load sharing between posterior elements and a stiff interbody spacer. This inconsistency may be explained by the displacement of the ICR. In axial rotation, where the highest load increment was reported, the ICR moved towards the centre of the disc, changing the motion pathway of the upper vertebra and, therefore the contact through the facet joints. In fact, when the cage was posteriorly placed the facet forces significantly decreased in all movements because the load was mainly transmitted through the implant.

Finally, cage subsidence risk has been predicted based on contact pressures [11], Von Misses stresses [8] and total reaction force [12]. However, none of these outcomes account for bone failure which is the actual cause of subsidence. In our study, the maximum pressures were similar to those obtained previously [11], but a constant

285   trend was not found with the variation of the cage design parameters. The irregularities of the endplates naturally

286   result in small contact areas with high loads, which may explain why the pressures did not show any trend when

287   varying the design. Thus, they hindered the discussion of which parameters will enhance subsidence resistance.

288   However, these pressures provoke stresses in the underlying bone which may cause inelastic strains.

289   To account for this inelastic behaviour, other authors used Von Mises equivalent stress as the criterion for bone

290   yielding. However, considering that the tensile strength of bone is smaller than its compressive strength, bone

291   should be treated as a brittle material and the Von Mises criteria would not be suitable [10]. Furthermore,

292   compressing collapse of crushable bone cells allowed for a gradual decrease of the stresses and a local hardening

293   of the tissue. This behaviour was studied by Kelly et al. [33] who proved that a crushable foam plasticity

294   formulation with pressure dependent yield behaviour provided the best approximation to the stress-strain curve

295   of the bone at a continuum level when compared with their results for a micro-FE model. Other studies [10,34]

296   have also shown that the Druker-Prager formulation is able to predict the post-yield behaviour of the bone that

297   can be improved by the definition of the hardening. In our model, the implementation of a modified Drucker-

298   Prager Cap plasticity material behaviour allowed to predict bone failure and, therefore, cage subsidence.

299   Contrary to other studies which found more inelastic strains in extension or lateral bending, in our model plastic

300   strains were more prone to occur in the anterior part of the caudal vertebra during flexion. This difference may

301   be related to the use of posterior fixation by Jalil et al. [35] which restricted the flexion motion decreasing the

302   compressive force on the anterior part of the endplates. Regarding the cage parameters, the inelastic strains

303   increased for cages with: high radius, high curvature and an anterior position. Thus, a wider cage reduced the

304   range of motion at the same time that increased the risk of subsidence, and the same occurred with an anteriorly

305   placed cage. So an equilibrium between segment stiffness and subsidence should be reached to determine the

306   best cage design. In agreement with our results, previous FE studies showed that a higher cage stiffness would

307   increase the risk of subsidence [11]. However, in contrast to our results, clinical studies have shown that a wider

308   cage increases the subsidence resistance [7,36] because they lay in the peripheral region where the structural

309   properties of the lumbosacral endplates are superior [37]. This disagreement is due to the fact that in this study

310   uniform properties have been considered for the bony structures due to the lack of material data. Lastly, in

311   extension, the yield zone moved backward to the vertebral arch and is mainly caused by tensile stresses. Here a

312   constant cortical thickness was considered for the entire vertebra, however, the arch has actually a thicker

313   cortical layer and, therefore, the stiffness of this part is higher and the inelastic strains would decrease.

314   It is noticeable that each cage design or positioning parameter was varied independently to determine those with

315   a higher influence on the surgical outcome, rather than to find and optimal design. To look for the optimal cage,

316   the interrelations would have to be taken into account and an optimization function would have to be defined

317   considering the compromise between segmental stiffness and bone integrity.

318   This study has a number of limitations. Firstly, we used a high friction coefficient at the cage-endplate interface,

319   assuming that the surfaces of the cages are prepared with a serrated geometry or roughness to avoid slippage of

320   the device [38]. Nevertheless, this parameter would be more important for the risk of cage migration than for

321   cage subsidence which is the goal of this work. Secondly, when modelling the mechanical behaviour of the

322   cartilaginous endplates linear elasticity and constant thickness were assumed. Modelling using a hyperelastic

323   material and irregular thickness would allow for a more accurate analysis of endplate behaviour. Regarding the

324   facet joints, the properties were taken in accordance with other previous studies, however, slight changes in the

325   gap distance, the degree of curvature or the facet orientation can lead to different results. In our study, the results

326   have been normalized with the intact data for comparison. In the model, the cage insertion canal was not

327   explicitly modelled. Given that the simulated surgery corresponded to a transforaminal lumbar interbody fusion

328   (TLIF) approach an anterolateral annular defect should have being included for a more actual prediction.

329   However, although it is expected to cause some asymmetry in the results, the largest part of the load was

330   transmitted through the cage and the posterior elements so it was assumed that the difference would not be

331   significant. Furthermore, the distraction of the segment due to the cage press-fit was not included. If the cage

332   height would be higher than the initial disc height, all the surrounding structures such as ligaments, muscles and

333   annular fibres would present a pre-strain which would increase the load in the cage and, therefore, the contact

334   pressures on the endplates. Nevertheless, considering that this pre-strain would affect all the cases, the predicted

335   trends with varying parameters is expected to be unaltered. For a more deep understanding of the effect of

336   segment distraction, a further parametric study should be performed varying cage height, and also considering

337   that the segment would adapt to the cage differently in each position depending on the specific geometry, so that

338   the pre-strain state of each structure would change from one to another. Furthermore, subsidence is directly

339   related to bone quality which must be cautiously evaluated preoperatively. In this model, the material properties

340   chosen for bone modelling corresponded with the lowest ones found in the literature [21] to create the worst

341   possible scenario. Moreover, they were considered uniform along the bony endplates. A characterization of the

342   local thickness and bone mineral density of the cortical and cancellous bone, derived from CT images via

343   Hounsfield unit translation into bone mineral density, would improve the subsidence prediction. Besides, as was

17

344 shown in other studies [39] the vertebral endplate morphology follows the bone remodelling principles. When an

345 implant is placed, the load sharing among the different regions of the endplate modified the mechanical

346 environment of the bone forming cells initiating a remodelling process which may lead to a new situation. In

347 further studies, the adaptive bone response to mechanical alterations should be studied in combination with its

348 inelastic behaviour. Finally, a quasistatic load was applied to cross compare among implants while the

349 physiologic environment of the lumbar segment would be better reproduced by a cyclic loading. It is expected

350 that the elements which underwent inelastic strains accumulate damage over time driving to the progressive

351 sinking of the implant into the vertebral body. Nevertheless, this study aims for the comparison between cage

352 designs, so it is expected that the higher the inelastic strains in the static case, the higher the accumulated damage

353 during time.

354 This model goes a step forward in subsidence prediction with the possibility to discern if the bone will fail under

355 the cage pressure or not. It was seen that cage design and placement played an important role in the

356 biomechanical behaviour of the FSU after lumbar surgery. A compromise between segment stiffness and bone

357 integrity should be reached by modifying the cross-sectional area, geometrical congruence and position of the

358 cage for each specific patient and each particular instrumentation. For that purpose, the model presented above

359 may be a useful tool for the preoperative evaluation of patient-specific surgery outcome. Having medical images

360 from the patient, it would be possible to segment the specific geometry and translate the Hounsfield units into

361 bone density information, allowing to test different instrumentations for this specific patient following the same

362 rationale. However, there are still aspects that should be included in order to construct accurate patient specific

363 models. For instance, the estimation of real muscle forces using optimization principles based on the range of

364 motion of that specific patient. Future researches could approach these issues.

365

366 **Conflict of interest statement**

367 The authors have not conflict of interest to declare.

368

369 **6. References**

370 [1] T.A. Zdeblick, F.M. Phillips, Interbody cage devices., Spine (Phila. Pa. 1976). 28 (2003) S2–7.

371 doi:10.1097/01.BRS.0000076841.93570.78.

372 [2] A. Ahmadian, K. Bach, B. Bolinger, G.M. Malham, D.O. Okonkwo, A.S. Kanter, J.S. Uribe, Stand-

373 alone minimally invasive lateral lumbar interbody fusion: Multicenter clinical outcomes, J. Clin.

374 Neurosci. 22 (2015) 740–746. doi:10.1016/j.jocn.2014.08.036.

375 [3] F. Costa, M. Sassi, A. Ortolina, A. Cardia, R. Assietti, A. Zerbi, M. Lorenzetti, F. Galbusera, M. Fornari,

376 Stand-alone cage for posterior lumbar interbody fusion in the treatment of high-degree degenerative disc

377 disease: Design of a new device for an "old" technique. a prospective study on a series of 116 patients,

378 Eur. Spine J. 20 (2011) 46–56. doi:10.1007/s00586-011-1755-0.

379 [4] E. Van de Kelft, J. Van Goethem, Trabecular metal spacers as standalone or with pedicle screw

380 augmentation, in posterior lumbar interbody fusion: a prospective, randomized controlled trial, Eur.

381 Spine J. 24 (2015) 2597–2606. doi:10.1007/s00586-015-4229-y.

382 [5] M. Panjabi, The stabilizing system of the spine. Part II. Neutral zone and instability hypothesis., J. Spinal

383 Disord. 5 (1992) 390–397.

384 [6] R.C. Mulholland, The myth of lumbar instability: The importance of abnormal loading as a cause of low

385 back pain, Eur. Spine J. 17 (2008) 619–625. doi:10.1007/s00586-008-0612-2.

386 [7] L. Marchi, N. Abdala, L. Oliveira, R. Amaral, E. Coutinho, L. Pimenta, Radiographic and clinical

387 evaluation of cage subsidence after stand-alone lateral interbody fusion., J. Neurosurg. Spine. 19 (2013)

388 110–1188. doi:10.3171/2013.4.SPINE12319.

389 [8] L.S. Chatham, V. V. Patel, C.M. Yakacki, R.D. Carpenter, Interbody Spacer Material Properties and

390 Design Conformity for Reducing Subsidence During Lumbar Interbody Fusion, J. Biomech. Eng. 139

391 (2017) 1–8. doi:10.1115/1.4036312.

392 [9] X. Liu, J. Ma, P. Park, X. Huang, N. Xie, X. Ye, Biomechanical comparison of multilevel lateral

393 interbody fusion with and without supplementary instrumentation: a three-dimensional finite element

394 study, BMC Musculoskelet. Disord. 18 (2017) 63. doi:10.1186/s12891-017-1387-6.

395 [10] M. Bessho, I. Ohnishi, J. Matsuyama, T. Matsumoto, K. Imai, K. Nakamura, Prediction of strength and

396 strain of the proximal femur by a CT-based finite element method, J. Biomech. 40 (2007) 1745–1753.

397   doi:10.1016/j.jbiomech.2006.08.003.

398   [11]   F. Galbusera, H. Schmidt, H.-J.J. Wilke, Lumbar interbody fusion: A parametric investigation of a novel

399   cage design with and without posterior instrumentation, Eur. Spine J. 21 (2012) 455–462.

400   doi:10.1007/s00586-011-2014-0.

401   [12]   C.C. Hsu, Shape optimization for the subsidence resistance of an interbody device using simulation-

402   based genetic algorithms and experimental validation, J. Orthop. Res. 31 (2013) 1158–1163.

403   doi:10.1002/jor.22317.

404   [13]   J. Cegoñino, V. Moramarco, A. Calvo-Echenique, C. Pappalettere, A. Pérez Del Palomar, A constitutive

405   model for the annulus of human intervertebral disc (IVD): implications for developing a degeneration

406   model and its influence on lumbar spine functioning, J. Appl. Math. 2014 (2014).

407   doi:10.1155/2014/658719.

408   [14]   M. Silva, C. Wang, T. Keaveny, H. WC, Direct and computed tomography thickness measurements of

409   the human, lumbar vertebral shell and endplate., Bone. 15 (1994) 409–414.

410   [15]   H. Schmidt, F. Galbusera, A. Rohlmann, T. Zander, H.J. Wilke, Effect of multilevel lumbar disc

411   arthroplasty on spine kinematics and facet joint loads in flexion and extension: A finite element analysis,

412   Eur. Spine J. 21 (2012) S663–S674. doi:10.1007/s00586-010-1382-1.

413   [16]   A. Castellvi, S. Thampi, D. Cook, M. Yeager, Y. Yao, Q. Zou, D. Whiting, M. Oh, E. Prostko, B. Cheng,

414   Effect of TLIF Cage Placement on In Vivo Kinematics, Int. J. Spine Surg. (2015) 1–7.

415   doi:10.14444/2038.

416   [17]   A. Abbushi, M. Cabraja, U.W. Thomale, C. Woiciechowsky, S.N. Kroppenstedt, The influence of cage

417   positioning and cage type on cage migration and fusion rates in patients with monosegmental posterior

418   lumbar interbody fusion and posterior fixation, Eur. Spine J. 18 (2009) 1621–1628. doi:10.1007/s00586-

419   009-1036-3.

420   [18]   S. Vadapalli, K. Sairyo, V.K. Goel, M. Robon, A. Biyani, A. Khandha, N. a Ebraheim, Biomechanical

421   rationale for using polyetheretherketone (PEEK) spacers for lumbar interbody fusion-A finite element

422   study., Spine (Phila. Pa. 1976). 31 (2006) E992–E998. doi:10.1097/01.brs.0000250177.84168.ba.

423   [19]   Y.M. Lu, W.C. Hutton, V.M. Gharpuray, Can variations in intervertebral disc height affect the

424   mechanical function of the disc?, Spine (Phila. Pa. 1976). 21 (1996) 2208–2217. doi:10.1097/00007632-

425   199610010-00007.

426   [20]   Y. Kim, Finite element analysis of anterior lumbar interbody fusion: threaded cylindrical cage and

427   pedicle screw fixation., Spine (Phila. Pa. 1976). 32 (2007) 2558–68.

428   doi:10.1097/BRS.0b013e318158cdd8.

429   [21]   D.L. Kopperdahl, T.M. Keaveny, Yield strain behavior of trabecular bone, J. Biomech. 31 (1998) 601–

430   608. doi:10.1016/S0021-9290(98)00057-8.

431   [22]   D. Lacroix, P.J. Prendergast, A mechano-regulation model for tissue differentiation during fracture

432   healing: Analysis of gap size and loading, J. Biomech. 35 (2002) 1163–1171. doi:10.1016/S0021-

433   9290(02)00086-6.

434   [23]   R. Eberlein, G. a. Holzapfel, C. a. J. Schulze-Bauer, An Anisotropic Model for Annulus Tissue and

435   Enhanced Finite Element Analyses of Intact Lumbar Disc Bodies, Comput. Methods Biomech. Biomed.

436   Engin. 4 (2001) 209–229. doi:10.1080/10255840108908005.

437   [24]   V. Moramarco, A. Pérez del Palomar, C. Pappalettere, M. Doblaré, An accurate validation of a

438   computational model of a human lumbosacral segment, J. Biomech. 43 (2010) 334–342.

439   doi:10.1016/j.jbiomech.2009.07.042.

440   [25]   J. Chazal, A. Tanguy, M. Bourges, G. Gaurel, G. Escande, M. Guillot, G. Vanneuville, Biomechanical

441   properties of spinal ligaments and a histological study of the supraspinal ligament in traction, J.

442   Biomech. 18 (1985) 167–176. doi:10.1016/0021-9290(85)90202-7.

443   [26]   F. Pintar, N. Yoganandan, T. Myers, Biomechanical properties of human lumbar spine ligaments, J.

444   Biomech. 25 (1992) 1351–1356.

445   [27]   F. Heuer, H. Schmidt, Z. Klezl, L. Claes, H.-J. Wilke, Stepwise reduction of functional spinal structures

446   increase range of motion and change lordosis angle, J. Biomech. 40 (2007) 271–280.

447   doi:10.1016/j.jbiomech.2006.01.007.

448   [28]   T. Zander, M. Dreischarf, A.-K. Timm, W.W. Baumann, H. Schmidt, Impact of material and

449   morphological parameters on the mechanical response of the lumbar spine — A finite element sensitivity

450   study, J. Biomech. 53 (2016) 185–190. doi:10.1016/j.jbiomech.2016.12.014.

451   [29]   V. Goel, M. Panjabi, A. Patwardhan, A. Dooris, H. Serhan, A.S. for T. and Materials, Test protocols for

452   evaluation of spinal implants, J. Bone Jt. Surg. Am. 88 (2006) 103–109. doi:10.2106/JBJS.E.01363.

453 [30] H.J. Wilke, K. Wenger, L. Claes, Testing criteria for spinal implants: recommendations for the

454 standarization of in vitro stability testing of spinal implants., Eur. Spine J. 7 (1998) 148–154.

455 [31] L. Pimenta, A.W.L. Turner, Z. a Dooley, R.D. Parikh, M.D. Peterson, Biomechanics of lateral interbody

456 spacers: going wider for going stiffer., Sci. World J. 2012 (2012) 6. doi:10.1100/2012/381814.

457 [32] T. Oxland, T. Lund, Biomechanics of stand-alone cages and cages in combination with posterior

458 fixation: a literature review, Eur. Spine J. 9 (2000) S095–S101.

459 [33] N. Kelly, N.M. Harrison, P. McDonnell, J.P. McGarry, An experimental and computational investigation

460 of the post-yield behaviour of trabecular bone during vertebral device subsidence, Biomech. Model.

461 Mechanobiol. 12 (2013) 685–703. doi:10.1007/s10237-012-0434-3.

462 [34] A. Phillips, P. Pankaj, F. May, K. Taylor, C. Howie, A. Usmani, Constitutive models for impacted

463 morsellised cortico-cancellous bone, Biomaterials. 27 (2006) 2162–2170.

464 doi:10.1016/j.biomaterials.2005.10.034.

465 [35] M.H. Jalil, M.H. Mazlan, M. Todo, Biomechanical Comparison of Polymeric Spinal Cages Using Ct

466 Based Finite Element Method, Int. J. Biosci. Biochem. Bioinforma. 7 (2017) 110–117.

467 doi:10.17706/ijbbb.2017.7.2.110-117.

468 [36] T. V Le, A. a. Baaj, E. Dakwar, C.J. Burkett, G. Murray, D. a. Smith, J.S. Uribe, Subsidence of

469 Polyetheretherketone Intervertebral Cages in Minimally Invasive Lateral Retroperitoneal Transpsoas

470 Lumbar Interbody Fusion, Spine (Phila. Pa. 1976). 37 (2012) 1268–1273.

471 doi:10.1097/BRS.0b013e3182458b2f.

472 [37] T.G. Lowe, S. Hashim, L. a Wilson, M.F. O'Brien, D. a B. Smith, M.J. Diekmann, J. Trommeter, A

473 biomechanical study of regional endplate strength and cage morphology as it relates to structural

474 interbody support., Spine (Phila. Pa. 1976). 29 (2004) 2389–2394.

475 doi:10.1097/01.brs.0000143623.18098.e5.

476 [38] S.-H. Chen, C.-L. Tai, C.-Y. Lin, P.-H. Hsieh, W.-P. Chen, Biomechanical comparison of a new stand-

477 alone anterior lumbar interbody fusion cage with established fixation techniques - a three-dimensional

478 finite element analysis., BMC Musculoskelet. Disord. 9 (2008). doi:10.1186/1471-2474-9-88.

479 [39] A. Agarwal, A.K. Agarwal, V.K. Goel, The Endplate Morphology Changes with Change in

480 Biomechanical Environment Following Discectomy, Int. J. Clin. Med. 04 (2013) 8–17.

481   doi:10.4236/ijcm.2013.47A1002.

482

483